

University of Nebraska - Lincoln

DigitalCommons@University of Nebraska - Lincoln

Biological Systems Engineering: Papers and
Publications

Biological Systems Engineering

7-6-2023

Assessing the impact of spatial resolution of UAS-based remote sensing and spectral resolution of proximal sensing on crop nitrogen retrieval accuracy

Kianoosh Hassani

Hamed Gholizadeh

Saleh Taghvaeian

Victoria Natalie

Jonathan Carpenter

See next page for additional authors

Follow this and additional works at: <https://digitalcommons.unl.edu/biosysengfacpub>



Part of the [Bioresource and Agricultural Engineering Commons](#), [Environmental Engineering Commons](#), and the [Other Civil and Environmental Engineering Commons](#)

This Article is brought to you for free and open access by the Biological Systems Engineering at DigitalCommons@University of Nebraska - Lincoln. It has been accepted for inclusion in Biological Systems Engineering: Papers and Publications by an authorized administrator of DigitalCommons@University of Nebraska - Lincoln.

Authors

Kianoosh Hassani, Hamed Gholizadeh, Saleh Taghvaeian, Victoria Natalie, Jonathan Carpenter, and Jamey Jacob

Assessing the impact of spatial resolution of UAS-based remote sensing and spectral resolution of proximal sensing on crop nitrogen retrieval accuracy

Kianoosh Hassani^a, Hamed Gholizadeh^a, Saleh Taghvaeian^b, Victoria Natalie^c, Jonathan Carpenter^d and Jamey Jacob^c

^aDepartment of Geography, Oklahoma State University, Stillwater, OK, USA; ^bBiological Systems Engineering Department, University of Nebraska-Lincoln, Lincoln, NE, USA; ^cDepartment of Mechanical and Aerospace Engineering, Oklahoma State University, Stillwater, OK, USA; ^dDepartment of Plant and Soil Sciences, Oklahoma State University, Stillwater, OK, USA

ABSTRACT

Foliar nitrogen (N) plays a central role in photosynthetic machinery of plants, regulating their growth rates. However, field-based methods for monitoring plant N concentration are costly and limited in their ability to cover large spatial extents. In this study, we had two objectives: (1) assess the capability of unoccupied aerial system (UAS) and non-imaging spectroscopic data in estimating sorghum and corn N concentration and (2) determine the impact of spatial and spectral resolution of reflectance data on estimating sorghum and corn N concentration. We used a UAS and an ASD spectroradiometer to collect canopy- and leaf-level spectral data from sorghum and corn at experimental plots located in Stillwater, Oklahoma, U.S. We also collected foliage samples in the field and measured foliar N concentration in the lab for model validation. To assess the impact of spectral scale on estimating N concentration, we resampled our leaf-level ASD data to generate datasets with coarser spectral resolutions. To determine the impact of spatial scale on estimating N concentration, we resampled our UAS data to simulate five datasets with varying spatial resolutions ranging from 5 cm to 1 m. Finally, we used a suite of vegetation indices (VIs) and machine learning algorithms (MLAs) to estimate N concentration. Results from leaf-level ASD spectral data showed that the resampled data matching the spectral resolution of our UAS-based data at five spectral bands ranging from 360 to 900 nm provided sufficient spectral information to estimate plot-level sorghum and corn N concentration. Regarding spatial resolution, canopy-level UAS data resampled at multiple pixel sizes, ranging from 1 cm to 1 m were consistently capable of estimating N concentration. Overall, our findings indicate the possibility of developing monitoring instruments with optimal spectral and spatial resolution for estimating N concentration in crops.


ARTICLE HISTORY

Received 5 December 2022
Accepted 6 July 2023

KEYWORDS

Unoccupied aerial system (UAS); spatial and spectral scale; crop nitrogen concentration; vegetation indices (VIs); machine learning algorithm (MLA); sorghum; corn

CONTACT Kianoosh Hassani  Kianoosh.hassani@okstate.edu  Department of Geography, Oklahoma State University, Stillwater, OK, USA

 Supplemental data for this article can be accessed online at <https://doi.org/10.1080/01431161.2023.2237162>.

© 2023 The Author(s). Published by Informa UK Limited, trading as Taylor & Francis Group.

This is an Open Access article distributed under the terms of the Creative Commons Attribution-NonCommercial-NoDerivatives License (<http://creativecommons.org/licenses/by-nc-nd/4.0/>), which permits non-commercial re-use, distribution, and reproduction in any medium, provided the original work is properly cited, and is not altered, transformed, or built upon in any way. The terms on which this article has been published allow the posting of the Accepted Manuscript in a repository by the author(s) or with their consent.

1. Introduction

N (nitrogen) is a vital macronutrient that is mainly invested in plants' photosynthesis-related proteins and chlorophyll pigments and promotes light use efficiency, carbon fixation, and photosynthetic activity of plants (Kokaly et al. 2009; Masclaux-Daubresse et al. 2010). Plants absorb N from soil in the form of ammonium and nitrate (Naftel 1931; Wright et al. 2004). Therefore, farmers apply N to their fields via fertilization to achieve optimal crop yield and quality (Beeckman, Motte, and Beeckman 2018). However, excessive fertilization leads to surplus N that leaches from soil into water resources and contributes to eutrophication of lakes and streams (Jaynes et al. 2001). Additionally, N over-fertilization stimulates nitrous oxide (N₂O) emissions from agricultural fields which have strong impact on global warming (Skiba and Rees 2014). In contrast, absence of sufficient N fertilization adversely affects plant photosynthetic assimilation and crop yield (Chlingaryan, Sukkarieh, and Whelan 2018; Milford et al. 1985). The economic consequences of reduced crop yield and quality due to plant N deficiency are not negligible (Hank et al. 2019). Thus, continuous monitoring of crop N concentration as a key plant trait would help farmers understand individual crop N requirements and provide an opportunity for improving crop yield and quality through site- and time-specific management practices (Weiss, Jacob, and Duveiller 2020).

Traditional approaches for monitoring plant N concentration involve *in-situ* plant sampling and laboratory-based analysis (Lynch and Barbano 1999). These approaches are costly, time- and labour-intensive, and their implementation across large fields are not often feasible. Instead, optical remote sensing has shown promise in estimating plant biochemical and physiological characteristics, including foliar N concentration (Hansen and Schjoerring 2003; Inoue, Darvishzadeh, and Skidmore 2018; Ustin and Gamon 2010). Nevertheless, the application of remote sensing data for estimating plant biochemical traits can be challenging, especially for crops as individual plants are much smaller than the spatial resolution (i.e. pixel size) of typical satellite and airborne remote sensing platforms. Previous studies have used satellite- and airborne-based remote sensing data with spatial resolution of several metres for the retrieval of plant N concentration (Boegh et al. 2002; Chen et al. 2010; Coops et al. 2003; Nigon et al. 2015). However, at such spatial resolutions, establishing relationships between plant spectral properties and biochemical traits is not straightforward since each pixel may contain different plant species, dead biomass, and soil. Thus, the application of remote sensing data with coarse spatial resolution, such as airborne and satellite data is limited if we are to estimate characteristics (i.e. traits) of individual plants such as N. To address the confounding issue of spatial scale, unoccupied aerial systems (UASs; also called drones) with fine spatial resolution have been successfully used to monitor and estimate plant N concentration across a variety of ecosystems (Jiang et al. 2020; Li et al. 2019; Näsi et al. 2018).

UASs are often equipped with multispectral cameras, which measure the electromagnetic radiation in only a few broad spectral bands within the visible (~400–700 nm), red-edge (~700–740 nm), and near-infrared (NIR; ~740–1300 nm) regions of the electromagnetic spectrum. However, the application of coarse spectral resolution multispectral data for estimating plant biochemical traits is often deemed limited since capturing subtle spectral absorption features of specific plant biochemical traits may require fine-resolution spectral data. In contrast, using hyperspectral data with a large number of

spectral bands and narrow bandwidth within the full spectrum (i.e. from 400 to 2500 nm) or visible near-infrared (VNIR; ~400 to 1300 nm) has shown promise in estimating plant N concentration (Kalacska, Lalonde, and Moore 2015; Pullanagari et al. 2021; Wang et al. 2013). Yet, due to technical constraints related to the design of imaging sensors, there is a trade-off between the spatial and spectral resolution of remote sensing data (Al-Wassai and Kalyankar 2013). Thus, satellite and airborne imaging spectrometers with fine spectral resolution are often characterized with coarser spatial resolution and therefore have limited capabilities for predicting vegetation biochemical traits. In this study, we tested the impact of spatial and spectral resolution of remotely sensed data for estimating sorghum and corn N concentration.

Remote sensing approaches, such as vegetation indices (VIs) and machine learning algorithms (MLAs) have shown success at estimating plant N concentration across different ecosystems. VIs combine information from several discrete spectral bands to develop relationships between plant spectral properties and its biochemical traits. For example, normalized difference vegetation index (NDVI) and red-edge-based indices including chlorophyll red-edge index (Clre) and red-edge inflection point index (REIP) are among the common indices that have been extensively used for estimating plant N concentration (Barzin et al. 2021; Hassani et al. 2023; He et al. 2016; Jay et al. 2017). Although simple VIs have yielded acceptable retrieval accuracies in estimating plant N concentration, using only a few spectral bands might weaken our ability to estimate N concentration, partly because spectral features that are used for estimating N are narrow or are distributed across different regions of the spectrum (Houborg, Fisher, and Skidmore 2015; Townsend et al. 2003). Furthermore, established relationships between VIs and plant N concentration can be site- and context-dependent and specific to the data used for model development, and therefore vary across crop types, growing stages, and environmental settings (Atzberger et al. 2011; Gholizadeh, Robeson, and Rahman 2015).

Such constraining factors in estimating plant N concentration can be mitigated using the entire available spectrum within the framework of MLAs or multivariate statistical approaches (Berger et al. 2020; Pullanagari et al. 2021). Several recent studies have provided evidence that different groups of MLAs or multivariate statistical approaches, including kernel-based algorithm (e.g. support vector regression (SVR); Cortes and Vapnik (1995)), ensemble learning (e.g. random forest; Rasmussen (2003)), and Bayesian algorithm (e.g. Gaussian process regression (GPR); Breiman (1996)), or partial least squares regression (PLSR) (Wold, Sjöström, and Eriksson 2001) often improve the N concentration estimation when compared with VIs (Liang et al. 2018; Miphokasap and Wannasiri 2018; Yao et al. 2015).

In this study, we assessed the capabilities of remotely sensed UAS data and proximal spectroradiometer data in estimating sorghum and corn N concentration (%) at different spatial and spectral resolutions. Specifically, we addressed two objectives: (1) assess the ability of UAS- and proximal spectroradiometer-derived metrics in estimating sorghum and corn N concentration over the growing season and (2) determine the impact of spatial and spectral resolutions on retrieval accuracy of sorghum and corn N concentration. We expected that finer spatial and spectral resolutions of spectral data can improve N concentration estimation for sorghum and corn. To achieve the specific objectives, we used UAS-mounted red-green-blue (RGB) and multispectral sensors and a proximal ASD FieldSpec 3 Standard

spectroradiometer (Analytical Spectral Devices, ASD, Malvern, UK) to collect spectral data from sorghum and corn at our experimental plots located in Stillwater, Oklahoma, U.S. For ground-truthing, we measured foliage N concentration through field sampling. To test the impact of spectral scale (i.e. spectral range, bandwidth, and the number of spectral bands), spectral measurements collected using the field spectroradiometer were used to simulate datasets with spectral resolutions of MicaSense RedEdge-MX multispectral UAS sensor, Sentinel 2-A, and Landsat 8 OLI. To test the impact of spatial scale, remotely sensed UAS datasets with spatial resolution of 1 cm were used to simulate additional datasets at coarser spatial resolutions (i.e. 5 cm, 10 cm, 25 cm, 50 cm, and 1 m). Finally, we used the original and simulated datasets to estimate sorghum and corn N concentration using VIs, MLAs, and PLSR. Findings from this work can potentially help identifying appropriate spatial and spectral resolutions for remote sensing of crop N concentration and developing rapid and efficient N monitoring systems.

2. Methods

2.1. Study site

We conducted our experiment at Efav site (36° 08'N, W 97° 06') in Stillwater, Oklahoma, U.S. The experiment period was the active sorghum and corn growing season from April to August 2020. The soil type of the experiment site was silty loam (fine-silty, mixed, super active, thermic fluventic Haplustolls). For each trial, five N treatment rates of 0, 50, 100, 150, and 200 kg/ha with four replications were applied prior to planting. For each crop, there were 20 plots (i.e. 40 plots in total) and the size of each plot was 3 m × 6 m with a spacing of 3 m between plots (Figure 1).

2.2. Data collection

2.2.1. Collecting leaf samples for plant N concentration quantification

We collected 800 sunlit top-of-canopy leaf samples from 40 plots during the growing season. Specifically, we collected ten leaf samples per plot during each field campaign, including the tillering and booting stages. We stored the samples in bags and transferred them to The Soil, Water, and Forage Analytical Laboratory (SWFAL) at Oklahoma State University. We then quantified N concentration (%) from 0.15 g of each leaf sample using a combustion analyser (Leco CN628, LECO Corporation, St. Joseph, Michigan, U.S.).

2.2.2. Leaf-level spectral sampling

We collected leaf-level spectral measurements within the 350–2500 nm range using an ASD FieldSpec 3 Standard spectroradiometer with a spectral resolution of 2 nm in the 350–1050 nm range and 10 nm in the 1050–2500 nm range. Leaf samples were placed on a black non-reflective surface and their spectral signatures were collected using the ASD spectroradiometer equipped with a contact leaf probe. We collected spectral measurements from the same plants that were used for N concentration sampling immediately after harvesting the leaf samples. For each leaf sample, three spectral measurements were taken from the leaf adaxial surface; each spectrum was the average of 30 readings. We re-

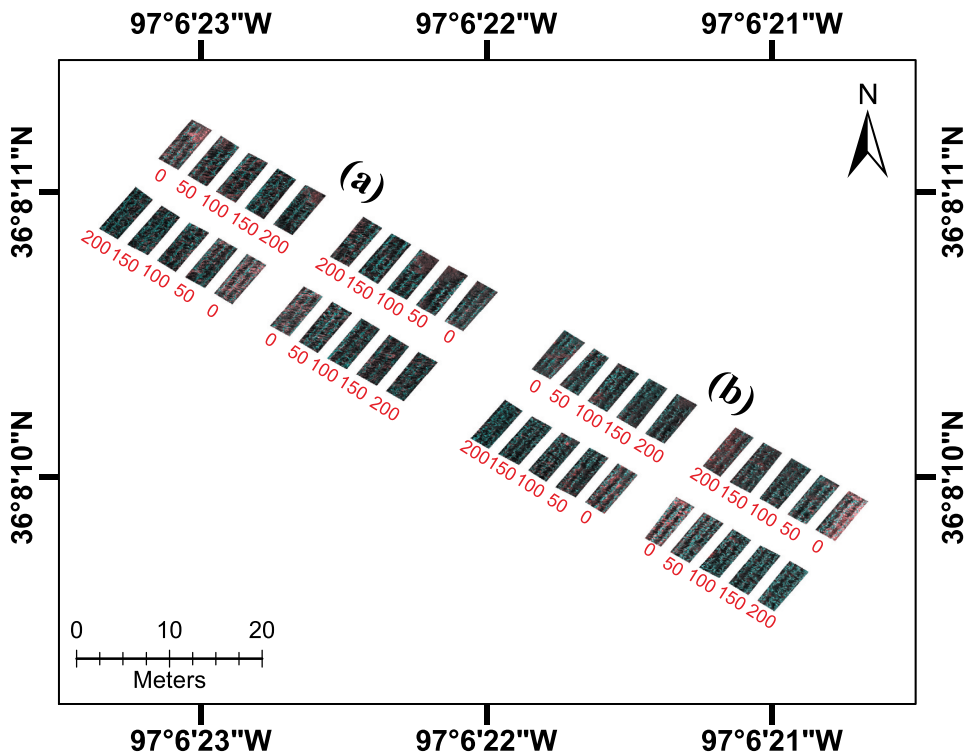


Figure 1. (A) Corn and (b) sorghum field trials within the Efav site (date of imagery: July 7, 2020). Red numbers below each plot represent pre-plant applied soil N treatment (kg/ha).

calibrated the spectroradiometer for dark current and referenced it to a white calibration panel every 10 minutes (Labsphere, North Sutton, New Hampshire, U.S.).

2.2.3. UAS data collection for spectral sampling

We conducted two flight missions on July 7 and August 20 in 2020 during clear-sky conditions and collected multispectral data from the study site. Both flights were conducted between 10:00 am (15:00 GMT) and 11:00 am local time (16:00 GMT). We used a DJI Matrice 600 Pro hexacopter equipped with a MicaSense RedEdge-MX sensor (MicaSense, Seattle, Washington, U.S.) to collect the multispectral data. The MicaSense RedEdge-MX had five 1.2 megapixel global-shutter single band cameras that imaged in the blue (centre wavelength 475 nm), green (centre wavelength 560 nm), red (centre wavelength 668 nm), red-edge (centre wavelength 717 nm), and NIR (centre wavelength 840 nm) spectral bands. The flights were planned using the Mission Planner software (3D Robotics, San Diego, CA, U.S.) and conducted at an altitude of approximately 30 m above ground level. The UAS images were acquired at 90% forward overlap and 60% side overlap. The final UAS multispectral images had a spatial resolution of 1 cm.

The UAS image preprocessing steps, including georeferencing, generation of orthomosaics, and radiometric correction of the multispectral data were performed in Agisoft Metashape software (Agisoft LLC., St. Petersburg, Russia). The process of generating

orthomosaics included the initial camera alignment, geometric correction, building dense point clouds, and production of multispectral orthomosaics. To improve the positional accuracy and model alignment of the UAS data, we established nine ground control points (GCPs) across the experimental site and recorded their coordinates using a Trimble R4 RTK (Trimble Inc., Sunnyvale, California, U.S.) global positioning system (GPS) receiver. We used two of our nine GCPs as check points to assess the accuracy of georeferencing. Finally, UAS radiance data were converted to reflectance using calibration tarps. Specifically, using an ASD FieldSpec 3 Standard spectroradiometer, spectral reflectance of six calibration panels, including black, blue, green, grey, red, and white were taken during the UAS flights. We used these data to calculate surface reflectance by applying the empirical line correction method (Conel et al. 1987).

2.3. Data analysis

2.3.1. Data simulation

Spectral resampling: For spectral resampling, we used the spectral response curve of each sensor, including the MicaSense RedEdge-MX, Sentinel 2-A, and Landsat 8 OLI and calculated the weighted average of the spectra from ASD spectroradiometer with the corresponding sensitivity factors derived from each sensor's spectral response curve as the weight. Following this procedure, we simulated the reflectance of each band for MicaSense RedEdge-MX, Sentinel 2-A, and Landsat 8 OLI sensors.

Spatial resampling: To assess the impact of spatial scale on estimating N concentration, we used the UAS-derived mosaics with spatial resolution of 1 cm to simulate reflectance datasets with coarser spatial resolutions at 5 cm, 10 cm, 25 cm, 50 cm, and 1 m through block averaging.

2.3.2. Estimating sorghum and corn N concentration using remote sensing metrics

We calculated three commonly used VIs, including NDVI, Clre, and REIP to estimate plant N concentration from our multispectral UAS, ASD, and both spectrally- and spatially-simulated datasets (Table 1). Additionally, we used linear regression, PLSR, and three MLAs, including SVR, GPR, and RF to estimate sorghum and corn N concentration from multispectral UAS, ASD, and both spectrally- and spatially-simulated datasets. In doing so, we assessed the performance of commonly used VIs compared to more complicated MLAs.

2.3.3. Assessing model performance

We assessed model performance of VIs using coefficient of determination (R^2) between the measured and estimated N concentration for the entire dataset containing 80 samples where relationships with $P < 0.05$ were considered significant. To assess the performance of MLAs and PLSR models, 60% of data were randomly selected and used for developing (or training) MLAs and PLSR models and the remaining 40% of the data were used for model validation. Specifically, the reflectance data from the ASD spectroradiometer and the spectrally-simulated datasets were used as the independent variables and sorghum and corn *in-situ* N concentration was used as the dependent variable. We repeated this process 100 times and used the average coefficient of determination and root mean square error (RMSE) of 100 runs to evaluate model performance. MLAs and PLSR models

Table 1. Definition of VIs used in this study. R, RE, and NIR represent reflectance in red, red-edge, and near-infrared bands of MicaSense RedEdge-MX multispectral UAS sensor, respectively.

Vegetation index	ASD FieldSpec 3	MicaSense RedEdge-MX multispectral UAS data	Sentinel 2-A	Landsat 8 OLI	Reference
Normalized difference vegetation index (NDVI)	$(R860 - R690)/(R860 + R690)$	$(NIR - R)/(NIR + R)$	$(B8 - B4)/(B8 + B4)$	$(B5 - B4)/(B5 + B4)$	(Rouse 1974)
Chlorophyll red-edge index (Clre)	$(R750/R710) - 1$	$(NIR/RE) - 1$	$(B8/B5) - 1$	No red-edge band	(Haboudane et al. 2002)
Red-edge inflection point index (REIP)	$700 + 40 \frac{R690-R700}{R740-R700}$	$700 + 40 \frac{RE-RE}{NIR-RE}$	$700 + 40 \frac{B4-B7-B5}{B6-B5}$	No red-edge band	(Guyot, Baret, and Major 1988)

were implemented in MATLAB 2020b (MathWorks Inc., Natick, Massachusetts, U.S.A.). For brevity, we are reporting results from the validation sets in the manuscript; results obtained from the training sets are reported in the Supplementary material.

2.3.4. Determining the contribution of different spectral regions in estimating N concentration

We also used PLSR coefficients and variable importance in projection (VIP) scores obtained from leaf-level ASD spectroradiometer data to determine the contribution of different wavelengths at estimating plant N concentration. Wavelengths with coefficients deviating from zero and VIP scores greater than 0.8 were considered important at predicting N concentration (Wold, Sjöström, and Eriksson 2001).

3. Results

3.1. Nitrogen concentration estimation using spectrally-resampled datasets

3.1.1. Sorghum N concentration estimation using VIs derived from spectrally-simulated datasets

We assessed the capability of three VIs, including NDVI, Clre, and REIP derived from the ASD spectroradiometer data and three spectrally-simulated datasets, including the simulated MicaSense RedEdge-MX multispectral UAS data, Sentinel 2-A, and Landsat 8 OLI (NDVI only) in estimating sorghum and corn N concentration. The relationships between VIs and estimated N concentration were determined for each dataset containing 40 samples and for each crop individually (Figure 2a–j; Fig. S1–4). For sorghum, our results showed that all VIs derived from spectrally-resampled leaf-level ASD data had positive and significant relationship with N concentration (Figure 2a–j). But red-edge-based indices, including REIP and Clre outperformed NDVI in estimating N concentration (Figure 2a–j). When using REIP, model performance (R^2) ranged from 0.68 (RMSE = 0.24%) for the spectrally-simulated UAS data to 0.72 (RMSE = 0.22%) for the spectrally-simulated Sentinel 2-A and ASD datasets (Figure 2a–c). When using Clre, the range of R^2 varied from 0.68 (RMSE = 0.24%) for the simulated Sentinel 2-A dataset to 0.72 (RMSE = 0.22%) for the simulated UAS dataset (Figure 2d–f). Additionally, the R^2 values for NDVI varied between 0.38 (RMSE = 0.33%) in the simulated Sentinel 2-A dataset and 0.43 (RMSE = 0.32%) in the simulated Landsat 8 OLI dataset (Figure 2g–j). The ASD data, in general, had a slightly better performance at estimating N concentration when compared to the spectrally-resampled datasets (Figure 2a and g).

3.1.2. Corn N concentration estimation using VIs derived from spectrally-simulated datasets

For corn, similar to sorghum, the results showed that VIs derived from the leaf-level ASD data and the spectrally-resampled datasets were capable of estimating corn N concentration (Figure 3a–j). Additionally, REIP and Clre had better performances than NDVI (Figure 3a–j). Specifically, REIP derived from the spectrally-simulated UAS data had the best performance ($R^2 = 0.81$ and RMSE = 0.21%; Figure 3a–c). For Clre, similar to REIP, the simulated UAS data showed the best performance ($R^2 = 0.85$ and RMSE = 0.18%;

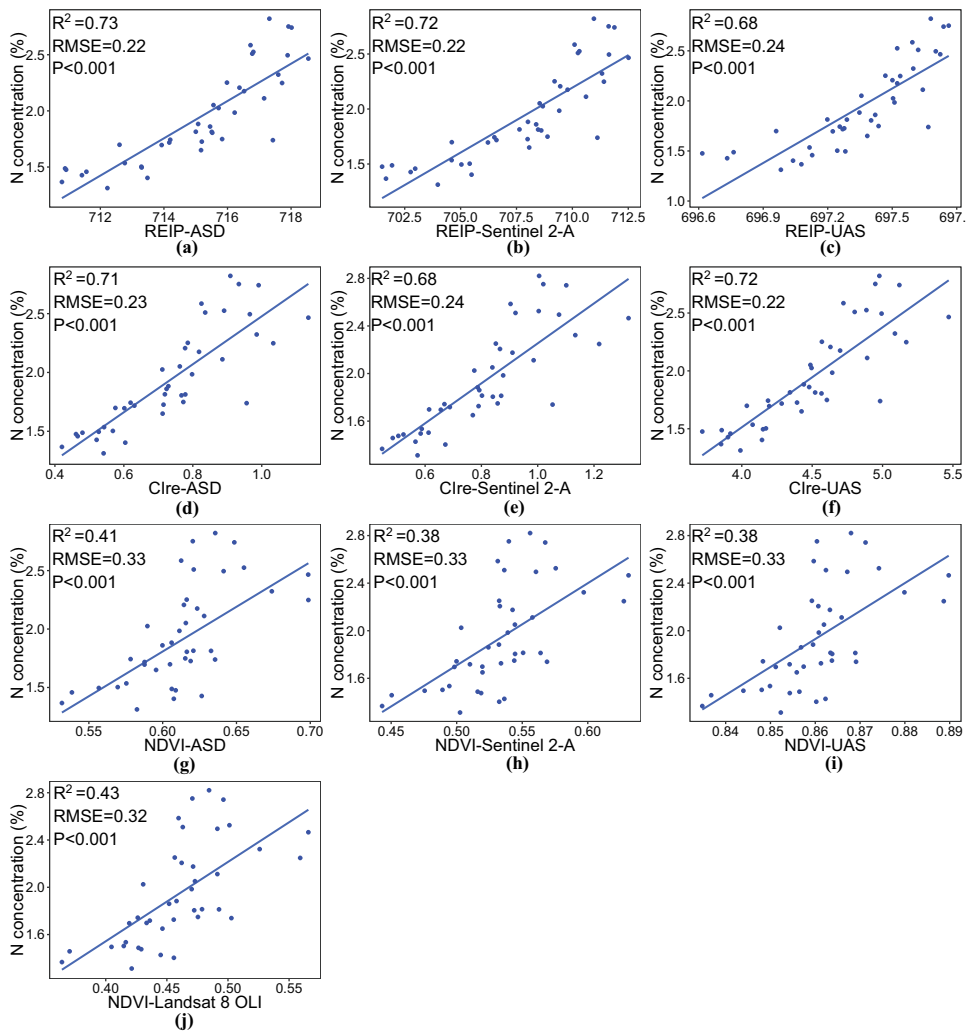


Figure 2. Predicted vs. observed sorghum N concentration (%) using (a-c) REIP, (d-f) Clre, and (g-j) NDVI based on the ASD and spectrally-simulated datasets, including Sentinel 2-A, UAS, and Landsat 8 OLI data (NDVI only). The blue lines correspond to the fitted line to the entire dataset containing 40 samples. Acronyms: REIP: red-edge inflection point index, Clre: chlorophyll red-edge index, NDVI: normalized difference vegetation index.

Figure 3d–f). When using NDVI, R^2 values ranged from 0.45 (RMSE = 0.36%) for the original ASD data to 0.55 (RMSE = 0.32%) for the simulated Landsat 8 OLI data (Figure 3g–j).

3.1.3. Sorghum N estimation using MLAs derived from spectrally-resampled datasets

When using the validation data set (40% of the data points permuted 100 times), all models, including linear regression and MLAs produced significant and positive associations with sorghum N concentration (Figure 4). Additionally, results from our leaf-level ASD data showed that using the resampled data matching the spectral resolution of the

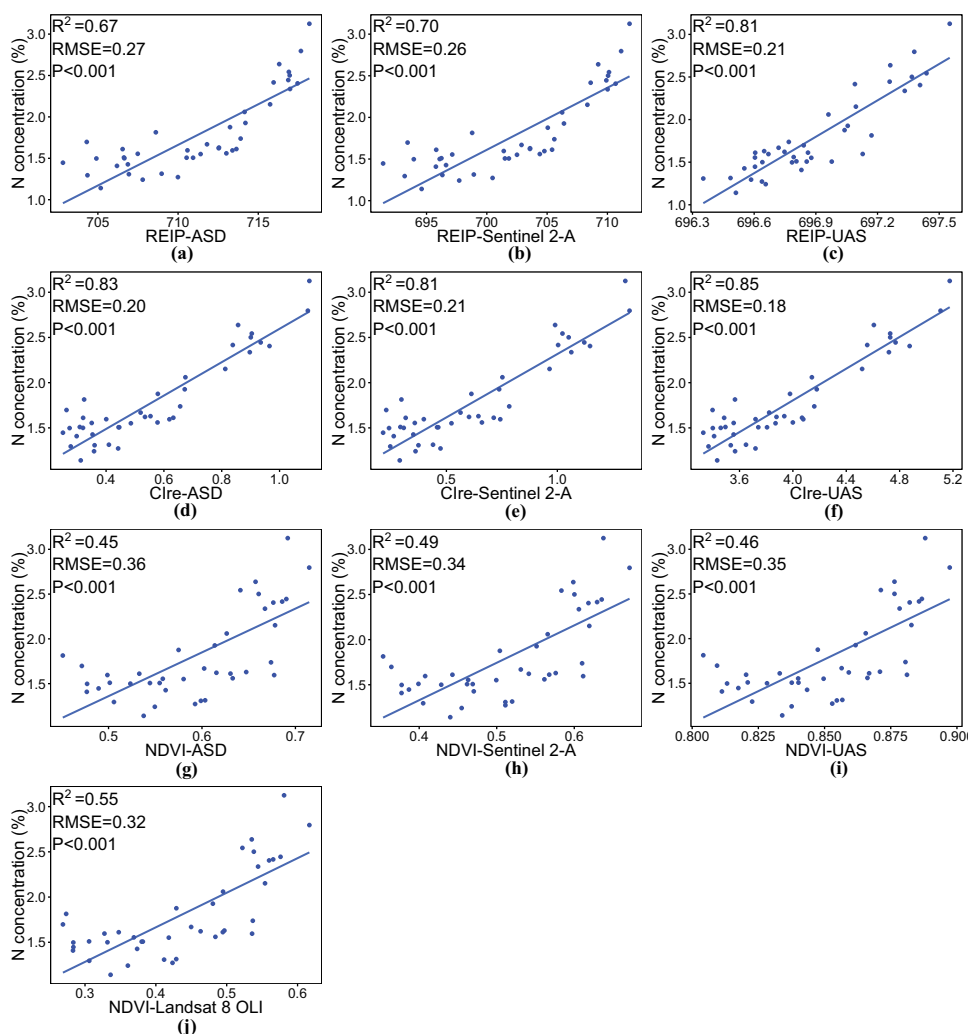


Figure 3. Predicted vs. observed corn N concentration (%) using (a–c) REIP, (d–f) Clre, and (g–j) NDVI based on the ASD and spectrally-simulated datasets, including the Sentinel 2-A, UAS, and Landsat 8 OLI data (NDVI only). The blue lines correspond to the fitted line to the entire dataset containing 40 samples. Acronyms: REIP: red-edge inflection point index, Clre: chlorophyll red-edge index, NDVI: normalized difference vegetation index.

UAS and Sentinel 2-A, in general, improved the retrieval accuracy of sorghum N concentration. Specifically, linear regression using all spectral bands and PLSR derived from the spectrally-simulated UAS data showed the highest coefficient of determination and lowest RMSE from 100 runs with R^2 of 0.83 ± 0.07 ($\text{RMSE} = 0.18 \pm 0.03\%$) and R^2 of 0.83 ± 0.04 ($\text{RMSE} = 0.19 \pm 0.04\%$), respectively (Figure 4; Table S1 and S2). Followed by these models, GPR derived from the spectrally-simulated Sentinel 2-A and UAS data showed the best predictive performances in terms of coefficient of determination and

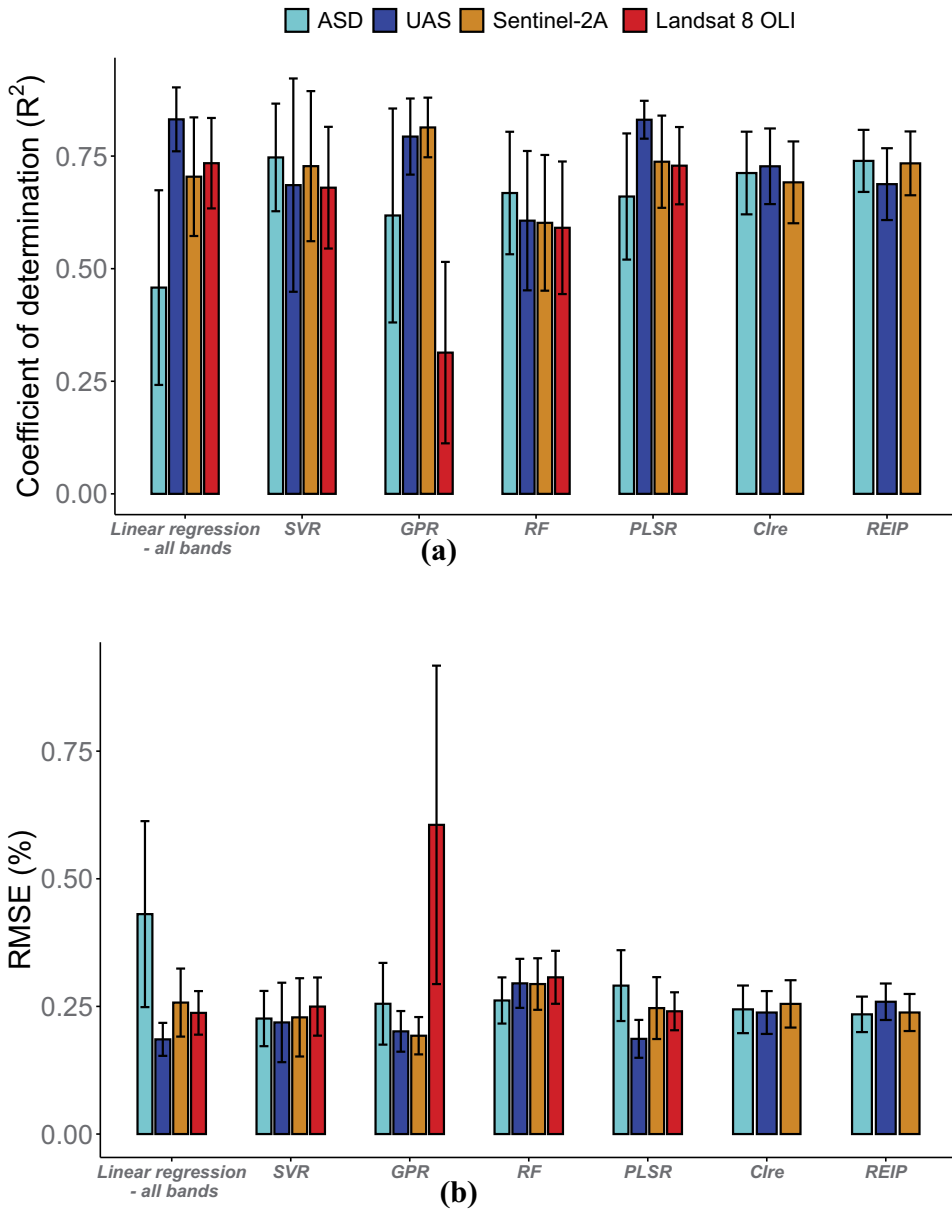


Figure 4. (A) Coefficient of determination (R^2) and (b) RMSE of estimated sorghum N concentration (%) using validation datasets. Vertical error bars show ± 1 standard deviation from 100 permutations. Acronyms: SVR: support vector regression, GPR: Gaussian process regression, RF: random forest, PLSR: partial least squares regression, Clre: chlorophyll red-edge index, REIP: red-edge inflection point index. In this figure, ASD refers to the original ASD data collected in the field, whereas the other three datasets are spectrally-resampled. Note: Since Landsat 8 OLI does not have a red-edge band, calculating Clre and REIP for OLI 8 was not possible.

RMSE with R^2 of 0.81 ± 0.07 ($\text{RMSE} = 0.19 \pm 0.04\%$) and R^2 of 0.79 ± 0.08 ($\text{RMSE} = 0.20 \pm 0.04\%$), respectively (Figure 4; Table S1 and S2). GPR model based on the spectrally-simulated Landsat 8 OLI data had the weakest agreement among all MLAs and showed the lowest R^2 and highest RMSE ($R^2 = 0.31 \pm 0.20$ and $\text{RMSE} = 0.61 \pm 0.31\%$; Figure 4; Table S1 and S2). Additionally, RF models based on the spectrally-resampled datasets had weak agreements with sorghum N concentration (Figure 4).

3.1.4. Corn N estimation using MLAs derived from spectrally-simulated datasets

Similar to sorghum, the results from corn validation data showed that all MLAs had positive and significant relationships with N concentration (Figure 5). Additionally, our results showed that the spectrally-resampled ASD data matching the spectral resolution of the UAS data outperformed other datasets in estimating corn N concentration. Specifically, GPR and linear regression derived from the simulated UAS data had the best performance based on corn N validation data with R^2 of 0.88 ± 0.05 ($\text{RMSE} = 0.17 \pm 0.04\%$) and R^2 of 0.85 ± 0.07 ($\text{RMSE} = 0.20 \pm 0.04\%$), respectively (Figure 5; Table S3 and S4). Further, PLSR model based on the spectrally-simulated UAS data had a strong association with corn N concentration ($R^2 = 0.81 \pm 0.07$ and $\text{RMSE} = 0.21 \pm 0.03\%$; Figure 5; Table S3 and S4). Linear regression-predicted N concentration based on the original leaf-level ASD data had the weakest agreement with corn N concentration validation data ($R^2 = 0.55 \pm 0.19$ and $\text{RMSE} = 0.45 \pm 0.14\%$; Figure 5; Table S3 and S4). Additionally, RF models derived from the spectrally-resampled datasets, in general, had the highest error rates compared with other MLAs (Figure 5b).

3.2. Contribution of different spectral regions at estimating N concentration based on leaf-level ASD data

For both sorghum and corn, PLSR coefficients at leaf-level ASD data showed different regions of the spectrum contributing to the estimation of N concentration (Figure 6a and c). Considering a threshold value of 0.8 for VIP values, the entire visible ($\sim 400\text{--}700\text{ nm}$) and red-edge bands ($\sim 700\text{--}740\text{ nm}$) were important at estimating sorghum and corn N concentration (Figure 6b and d). Additionally, for both sorghum and corn, only a few regions of NIR ($\sim 740\text{--}1100\text{ nm}$) and shortwave infrared ($\sim 1100\text{--}2450\text{ nm}$) were important at estimating N concentration (Figure 6a–d).

3.3. N concentration estimation using spatially-simulated datasets

3.3.1. N concentration estimation using VIs derived from spatially-simulated datasets

The relationships between VIs (i.e. NDVI, Clre, and REIP) and estimated N concentration were determined for each spatially-simulated dataset containing 40 samples and for each crop individually (Figure 7a,b). Our results showed that canopy-level UAS data resampled at multiple pixel sizes, ranging from 1 cm to 1 m, were consistently capable of estimating sorghum N concentration (Figure 7a). Specifically, Clre and NDVI had positive and significant relationships with N concentration using the original UAS data and spatially-

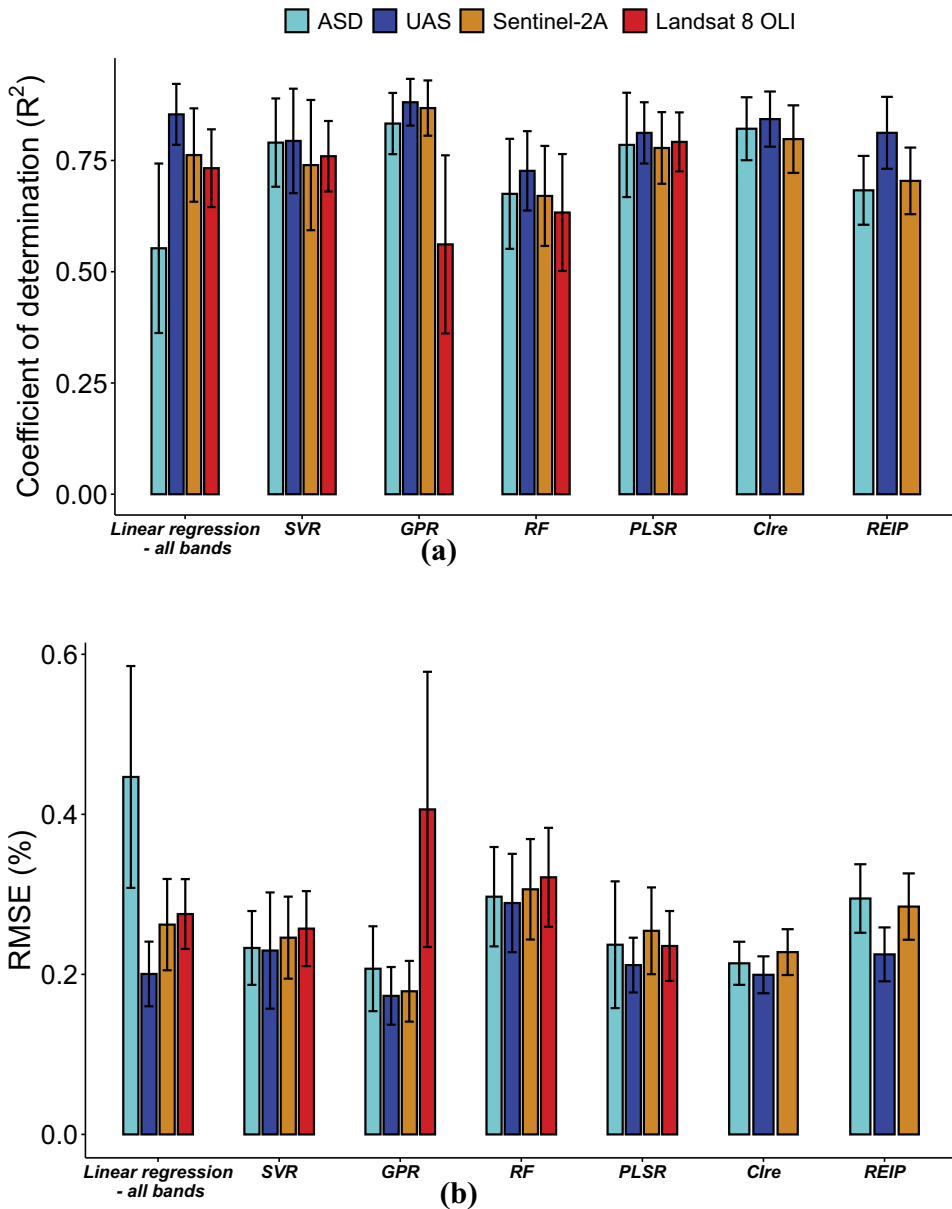


Figure 5. (A) Coefficient of determination (R^2) and (b) RMSE of estimated corn N concentration (%) using validation datasets. Vertical error bars show ± 1 standard deviation from 100 permutations. Acronyms: SVR: support vector regression, GPR: Gaussian process regression, RF: random forest, PLSR: partial least squares regression, Clre: chlorophyll red-edge index, REIP: red-edge inflection point index. In this figure, ASD refers to the original ASD data collected in the field, whereas the other three datasets are spectrally-resampled. Note: Since Landsat 8 OLI does not have a red-edge band, calculating Clre and REIP for OLI 8 was not possible.

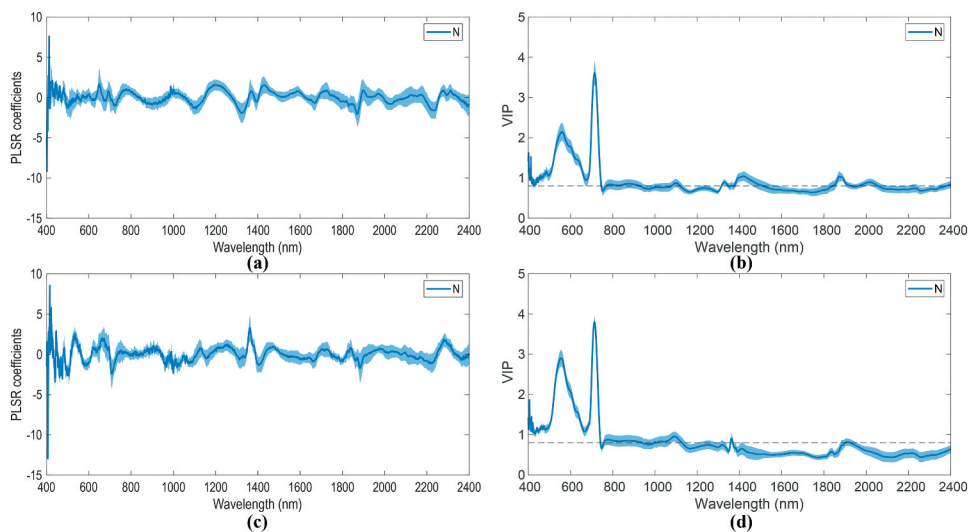


Figure 6. PLSR coefficients and variable importance in projection (VIP) scores obtained from sorghum (a-b) and corn (c-d) leaf-level ASD data using the validation datasets. Independent variables are ASD reflectance data and dependent variables are leaf-level N concentration (%). Shaded areas show ± 1 standard deviation from 100 permutations. Functional trait acronyms: N: nitrogen.

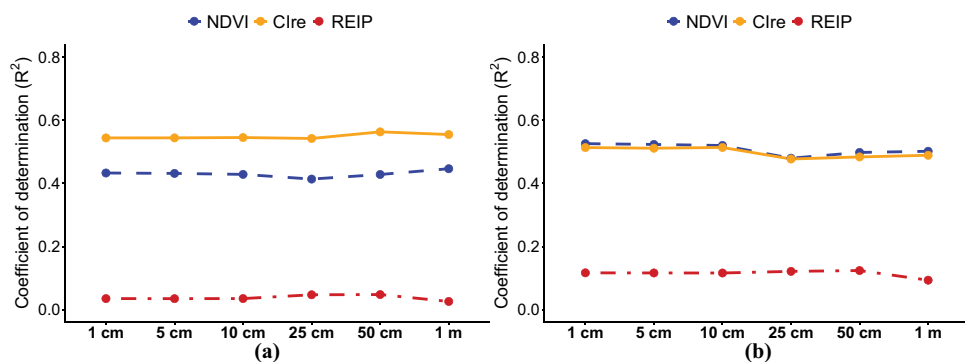


Figure 7. Coefficient of determination (R^2) of estimated N concentration for sorghum (a) and corn (b) using NDVI, Clre, and REIP derived from the original UAS data at spatial resolution of 1 cm and spatially-simulated datasets at spatial resolutions of 5 cm, 10 cm, 25 cm, 50 cm, and 1 m. Acronyms: NDVI: normalized difference vegetation index, Clre: chlorophyll red-edge index, REIP: red-edge inflection point index.

simulated datasets (Figure 7a). Additionally, Clre outperformed NDVI in estimating sorghum N concentration using the original UAS data and spatially-simulated datasets. No significant associations were found between REIP and sorghum N concentration using the spatially-resampled datasets (Figure 7a). Our results showed that the performance of

resampled canopy-level UAS data at coarser spatial resolution were comparable to those resampled at finer spatial resolutions.

For corn, similar to sorghum, our results showed that spatially-resampled canopy-level UAS data ranging from 1 cm to 1 m were consistently capable of estimating N concentration (Figure 7b). Specifically, Clre and NDVI derived from the original UAS data and spatially-simulated datasets showed strong and similar relationships with N concentration (Figure 7b). There were no significant relationships between REIP and corn N concentration across all spatial resolutions. Overall, our results showed that the performance of our canopy-level UAS data did not weaken after resampling to coarser pixel sizes, such as 50 cm and 1 m.

3.3.2. N concentration estimation using MLAs derived from spatially-simulated datasets

Using linear regression and MLAs produced significant and positive associations with sorghum N concentration based on the original UAS data and spatially-simulated

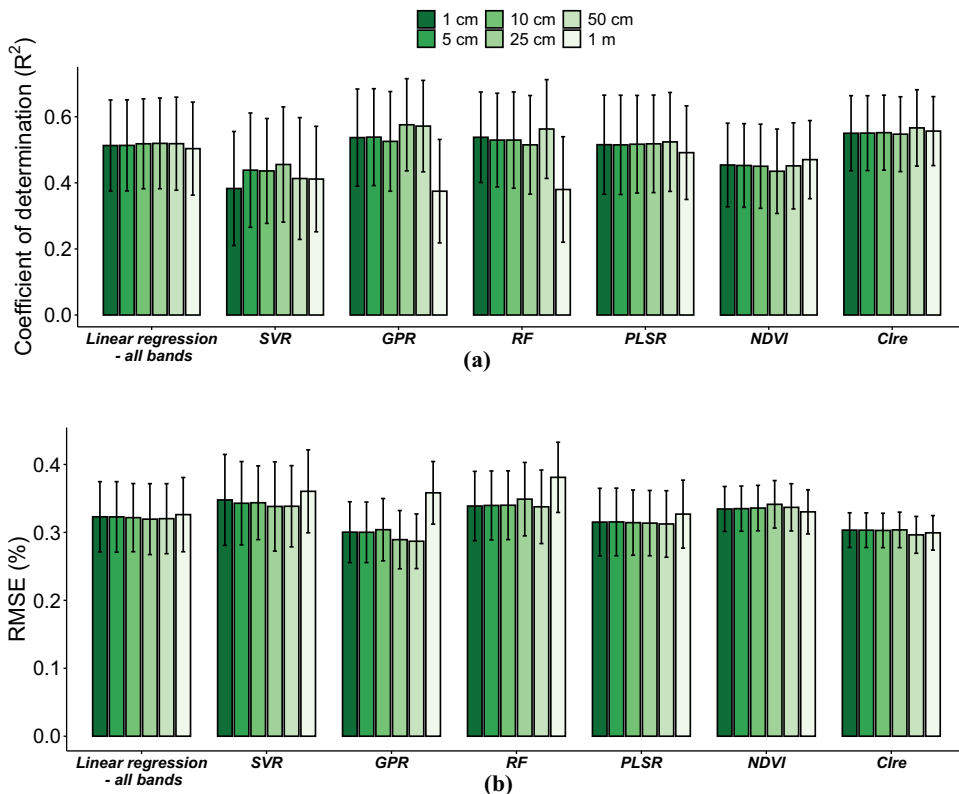


Figure 8. (A) Coefficient of determination (R^2) and (b) RMSE of estimated sorghum N concentration (%) derived from the original UAS data at spatial resolution of 1 cm and spatially-simulated datasets at spatial resolutions of 5 cm, 10 cm, 25 cm, 50 cm, and 1 m. Vertical error bars show ± 1 standard deviation from 100 permutations. Acronyms: SVR: support vector regression, GPR: Gaussian process regression, RF: random forest, PLSR: partial least squares regression, NDVI: normalized difference vegetation index, Clre: chlorophyll red-edge index.

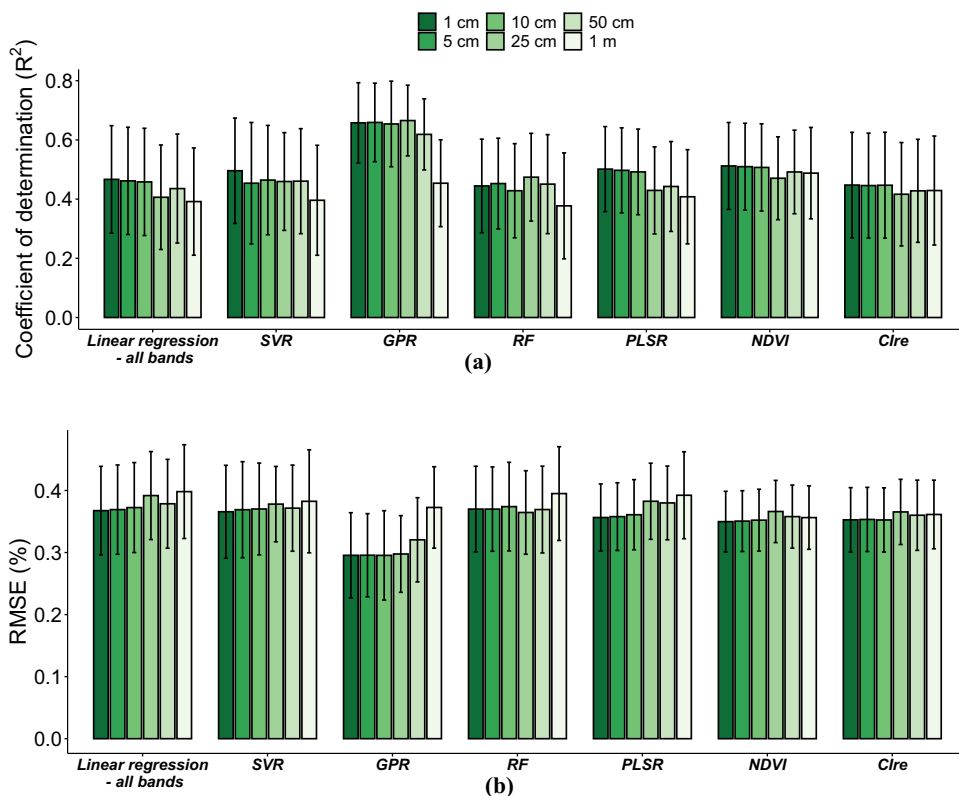


Figure 9. (A) Coefficient of determination (R^2) and (b) RMSE of estimated corn N concentration (%) derived from the original UAS data at spatial resolution of 1 cm and spatially-simulated datasets at spatial resolutions of 5 cm, 10 cm, 25 cm, 50 cm, and 1 m. Vertical error bars show ± 1 standard deviation from 100 permutations. Acronyms: SVR: support vector regression, GPR: Gaussian process regression, RF: random forest, PLSR: partial least squares regression, NDVI: normalized difference vegetation index, Clre: chlorophyll red-edge index.

datasets (Figure 8). Specifically, GPR derived from the spatially-simulated UAS data at 25 cm ($R^2 = 0.58 \pm 0.14$ and $\text{RMSE} = 0.29 \pm 0.04\%$) and 50 cm ($R^2 = 0.57 \pm 0.14$ and $\text{RMSE} = 0.29 \pm 0.04\%$) and RF model at 50 cm (R^2 of 0.56 ± 0.15 and RMSE of $0.34 \pm 0.05\%$) showed the highest coefficient of determination and lowest RMSEs from 100 runs (Figure 8; Table S5 and S6). GPR model derived from the spatially-simulated UAS data at 1 m had the weakest agreement with corn N concentration among all MLAs in terms of coefficient of determination and RMSE ($R^2 = 0.39 \pm 0.16$ and $\text{RMSE} = 0.35 \pm 0.05\%$; Figure 8; Table S5 and S6). Additionally, SVR models based on the spatially-simulated datasets had weak agreements with sorghum N concentration (Figure 8; Table S5 and S6). Overall, these results showed that at coarser spatial resolutions, such as 25 and 50 cm, the canopy-level UAS data were still able to successfully estimate sorghum N concentration.

Similar to sorghum, the results from corn validation data showed that linear regression and MLAs had positive and significant relationships with N concentration based on the original and spatially-simulated UAS datasets (Figure 9). Specifically, GPR models derived from the spatially-simulated UAS data ranging from 1 cm to 50 cm outperformed other models with R^2 ranging from 0.62 ± 12 ($\text{RMSE} = 0.32 \pm 0.07\%$) to 0.66 ± 12 ($\text{RMSE} = 0.30 \pm 0.06\%$) (Figure 9; Table S7 and S8). Further, PLSR results obtained from the canopy-level UAS data resampled at 1 cm ($R^2 = 0.50 \pm 0.14$ and $\text{RMSE} = 0.36 \pm 0.05\%$) and 5 cm ($R^2 = 0.50 \pm 0.14$ and $\text{RMSE} = 0.36 \pm 0.05\%$) showed strong associations with corn N concentration (Figure 9; Table S7 and S8). RF model derived from the spatially-simulated UAS data at 1 m had the weakest agreement with corn validation data ($R^2 = 0.38 \pm 0.18$ and $\text{RMSE} = 0.40 \pm 0.08\%$; Figure 9; Table S7 and S8).

4. Discussion

4.1. *Very fine spectral and spatial resolution data may not be necessary for crop N concentration estimation*

4.1.1. *Impact of spectral resolution on estimating N concentration*

Although spectral resolution is known to affect plant N concentration retrieval accuracy (Pullanagari et al. 2021; Wang et al. 2020), our results showed that finer spectral resolution data did not necessarily improve retrieval accuracies for sorghum and corn N concentration (Figure 4 and 5). For instance, using VIs, in general, provided similar or better retrieval accuracy than when using all spectral bands (Figure 4 and 5). Additionally, the results from our leaf-level ASD data showed that all spectrally-resampled datasets had comparable performances (Figure 4 and 5). Based on these results, we conclude that the sensor design (i.e. number and placement of spectral bands and Full Width at Half Maximum (FWHM) of each spectral band) did not affect N retrieval accuracy and our resampled datasets were capable of estimating N concentration as long as they had specific spectral bands, including the visible, red-edge, and NIR bands. Our PLSR results, further confirmed these findings and showed that, the wavelengths in PAR, red-edge, and a few regions in NIR contained the most important features for estimating sorghum and corn N concentration (Figure 6a–6). We, therefore, argue that UASs with five spectral bands (i.e. blue, green, red, NIR, and red-edge) from 360 to 900 nm can provide sufficient and reliable spectral information to operationally estimate plot-level sorghum and corn N concentration.

4.1.2. *Impact of spatial scale of remote sensing data on estimating N concentration*

Previous studies underpinned the importance of spatial resolution of remote sensing data in estimating foliar N concentration (Jiang et al. 2020; Näsi et al. 2018). For instance, Zhou et al. (2018) showed that the ability of remotely sensed data to estimate N concentration in paddy rice decreased at coarse spatial resolutions. Our results showed that canopy-level UAS data resampled at multiple pixel sizes, ranging from 1 cm to 1 m, were able to successfully estimate sorghum and corn N concentration and therefore, plot-level estimation of sorghum and corn in our experiment was not dependent on spatial scale of remote sensing data (Figure 7, 8, 9). Specifically, in our experiment, we observed that the performance of resampled UAS data at coarser spatial resolutions was comparable to those

resampled at finer spatial resolutions (R^2 ranging between approximately 0.35 and 0.65; [Figures 7, 8, 9](#)), showing that at plot-level, estimation of sorghum and corn N concentration with moderate spatial resolution data was possible likely due to the homogeneity of our study site and low structural complexity. Based on these findings, we conclude that in homogeneous plant communities, spatial resolution plays a less important role at estimating crop N concentration as opposed to heterogeneous landscapes. Overall, our experiment showed that multispectral UAS data over a range of fine to moderate spatial resolutions were capable of estimating sorghum and corn N concentration.

4.2. Key spectral regions in estimating sorghum and corn N concentration

Our results showed that the majority of wavelengths in visible and red-edge regions were important for estimating sorghum and corn N concentration ([Figure 6a–d](#)). In addition, a few wavelengths in NIR and shortwave infrared regions contributed to estimating sorghum and corn N concentration ([Figure 6a–d](#)). We note that N does not have specific spectral absorption features and presume that the selection of bands within the PAR region (~400–700 nm) may be related to absorption features of N-containing pigments, including chlorophyll and other photosynthetic pigments such as carotenoids (Curran 1989; Gholizadeh et al. 2022; Kokaly and Skidmore 2015). Specifically, we identified wavelengths near 430 nm and 660 nm as important regions for estimating N in sorghum and corn ([Figure 6a–d](#)) which are consistent with known absorption features of chlorophyll within the PAR region (Curran 1989; Du et al. 1998; Ustin et al. 2009). Additionally, important wavelengths within the 450–480 nm range ([Figure 6a–d](#)) matched with known absorption features of carotenoids (Du et al. 1998; Kokaly and Skidmore 2015; Ustin et al. 2009).

In addition to PAR region, the wavelengths in red-edge region were important at estimating sorghum and corn N concentration ([Figure 6a–d](#)). The importance of red-edge region at retrieving N concentration has been reported in previous studies (Clevers and Gitelson 2013; Wang et al. 2020). Our leaf-level PLSR models exhibited some of these important features, including the feature near 710 nm ([Figure 6a–d](#)). Additionally, some important wavelengths in NIR and shortwave infrared regions for estimating N concentration of sorghum and corn, such as features near 770 nm, 1730 nm, and 2300 nm ([Figure 6a and c](#)) were consistent with known absorption features of lignin, protein, and cellulose (Curran 1989; Fourty et al. 1996; Wang et al. 2020). This could be, in part, due to associations between plant N concentration and other biochemical components, including lignin, protein, and cellulose (Kokaly et al. 2009; Wang et al. 2020).

4.3. Optimal remote sensing metrics for estimating sorghum and corn N concentration

Based on our results, the choice of remote sensing metrics largely impacts the performance of remote sensing data when quantifying N concentration. VIs derived from our remote sensing data were able to successfully estimate crop N concentration. Specifically, our findings showed that sorghum and corn N concentration had stronger associations with red-edge-based indices, including Clre and REIP derived from non-imaging spectroscopic data ([Figure 2 and 3](#)). The stronger performance of red-edge-based VIs in

estimating plant N concentration has been reported in previous studies and was discussed in [Section 4.2](#) (Barzin et al. 2021; He et al. 2016; Jay et al. 2017).

We also note that previous work has suggested that combining all spectral bands within the framework of MLAs provides supplemental information regarding the impact of crop structural properties as well as other biochemical properties that are related to N concentration (Kokaly et al. 2009; Wang et al. 2020). However, we observed no significant improvements in estimating N concentration when using MLAs and linear regression with all spectral bands, likely due to information redundancy and multicollinearity between bands.

Overall, our findings provided evidence that using red-edge-based VIs, in most cases, yielded similar or stronger performance for predicting sorghum and corn N concentration. Thus, we argue that these relatively simple VIs can be reliably used as alternatives to MLAs for estimating plot-level sorghum and corn N concentration, especially when developing MLAs requires multiple extensive *in-situ* data collection campaigns to properly represent variations in crop status and environmental conditions during the growing season.

4.4. Limitations and future research

Crop phenology – the temporal variations in crop physiological traits, such as N concentration due to plants life-cycle events – was not considered in this study mainly because the significant cost of field data collections and laboratory-based N analysis limited our ability to repeat our data collection campaigns over time. Conducting our experiment at one point in time is one of the limitations of our study. Studies based on *in-situ* measurements have provided ample evidence that crops foliar N concentration and their response to soil N vary over time both within and between years (Raun et al. 2019). During warm and moist seasons, and with concurrent increase in soil microorganisms, N mineralization rate (i.e. conversion of N in soil organic matter into inorganic ammonium and nitrate) increases. Increases in N mineralization rate will, in turn, enhance crop N concentration and lower crop dependence on N fertilizer (White et al. 2021). These temporal variations in N concentration can potentially affect the quantification of N concentration using remotely sensed data as shown in previous remote sensing studies (Hassani et al. 2023; Ustin and Gamon 2010).

There is a critical need for continuous monitoring of crop N concentration during different crop developmental stages and over the years to understand crop N requirements and provide time-specific N management practices; conducting multi-temporal remote sensing experiments is essential to understand the impact of phenology and environmental variables on crop N concentration.

Our experiment was limited to one site which might limit the transferability of our results to other sites. In addition to climate conditions, site characteristics and management practices play important roles in crop foliar N concentration and crop N demand (Lollato et al. 2019). No-till farming and crop rotations have shown to greatly impact the amount of N available to crops (Arnall, Edwards, and Godsey 2008) and the capability of remote sensing to estimate crop N concentration can vary significantly depending on site characteristics. As a result, expanding the current experiment to other sites with different management practices can be an interesting future research path.

5. Conclusion

Traditional field-based methods for monitoring crop N concentration are expensive and implementing them for large field trials is not straightforward. Instead, optical remote sensing has shown promise in estimating plant N concentration. However, the choice of the optimal spatial and spectral resolution and the best remote sensing metric to estimate plant N concentration still remains elusive. In this study, we examined the capability of UAS and non-imaging spectroscopic spectral data for estimating sorghum and corn N concentration at different spectral and spatial resolutions over the growing season. Regarding the spectral resolution, our experiment showed that the resampled leaf-level ASD data at five spectral bands ranging from 360 to 900 nm, in general, can be reliably used for estimating plot-level sorghum and corn N concentration. Regarding spatial resolution, our resampled canopy-level UAS data showed that coarse spatial resolution data at 50 cm are capable of estimating sorghum and corn N concentration. These findings can potentially contribute to the development of low-cost sensors with optimal spatial and spectral resolution for estimating N concentration of crops.

Acknowledgements

We sincerely thank three anonymous reviewers who helped us improve the quality of our manuscript. We also express our sincere gratitude to Dr. William Raun for his invaluable help during this project.

Disclosure statement

No potential conflict of interest was reported by the author(s).

ORCID

Kianoosh Hassani  <http://orcid.org/0000-0001-9667-9211>

Data availability statement

The data that support the findings of this study are available from the corresponding author upon request by email: Kianoosh.hassani@okstate.edu.

References

- Al-Wassai, F. A., and N. Kalyankar. 2013. "Major Limitations of Satellite Images." *Journal of Global Research in Computer Science* 5 (4): 51–59.
- Arnall, D. B., J. T. Edwards, and C. B. Godsey. 2008. *Reference Strip Series: Applying Your Nitrogen-Rich and Ramp Calibration Strips*. Stillwater, OK, USA: Oklahoma Cooperative Extension Service.
- Atzberger, C., K. Richter, F. Vuolo, R. Darvishzadeh, and M. Schlerf. 2011. "Why Confining to Vegetation Indices? Exploiting the Potential of Improved Spectral Observations Using Radiative Transfer Models. In C. M. U. Neale & A. Maltese (Eds.), *Remote Sensing for Agriculture, Ecosystems, and Hydrology XIII*, Vol. 8174, 263–278. Prague, Czech Republic: SPIE.

- Barzin, R., H. Lotfi, J. J. Varco, and G. C. Bora. 2021. "Machine Learning in Evaluating Multispectral Active Canopy Sensor for Prediction of Corn Leaf Nitrogen Concentration and Yield." *Remote Sensing* 14 (1): 120. <https://doi.org/10.3390/rs14010120>.
- Beeckman, F., H. Motte, and T. Beeckman. 2018. "Nitrification in Agricultural Soils: Impact, Actors and Mitigation." *Current Opinion in Biotechnology* 50:166–173. <https://doi.org/10.1016/j.copbio.2018.01.014>.
- Berger, K., J. Verrelst, J.-B. Féret, T. Hank, M. Wochoer, W. Mauser, and G. Camps-Valls. 2020. "Retrieval of Aboveground Crop Nitrogen Content with a Hybrid Machine Learning Method." *International Journal of Applied Earth Observation and Geoinformation* 92:102174. <https://doi.org/10.1016/j.jag.2020.102174>.
- Boegh, E., H. Soegaard, N. Broge, C. Hasager, N. Jensen, K. Schelde, and A. Thomsen. 2002. "Airborne Multispectral Data for Quantifying Leaf Area Index, Nitrogen Concentration, and Photosynthetic Efficiency in Agriculture." *Remote Sensing of Environment* 81 (2–3): 179–193. <https://doi.org/10.1016/S0034-42570100342-X>.
- Breiman, L. 1996. "Bagging Predictors." *Machine Learning* 24 (2): 123–140. <https://doi.org/10.1007/BF00058655>.
- Chen, P., D. Haboudane, N. Tremblay, J. Wang, P. Vigneault, and B. Li. 2010. "New Spectral Indicator Assessing the Efficiency of Crop Nitrogen Treatment in Corn and Wheat." *Remote Sensing of Environment* 114 (9): 1987–1997. <https://doi.org/10.1016/j.rse.2010.04.006>.
- Chlingaryan, A., S. Sukkariéh, and B. Whelan. 2018. "Machine Learning Approaches for Crop Yield Prediction and Nitrogen Status Estimation in Precision Agriculture: A Review." *Computers and Electronics in Agriculture* 151:61–69. <https://doi.org/10.1016/j.compag.2018.05.012>.
- Clevers, J. G., and A. A. Gitelson. 2013. "Remote Estimation of Crop and Grass Chlorophyll and Nitrogen Content Using Red-Edge Bands on Sentinel-2 And-3." *International Journal of Applied Earth Observation and Geoinformation* 23:344–351. <https://doi.org/10.1016/j.jag.2012.10.008>.
- Conel, J. E., R. O. Green, G. Vane, C. J. Bruegge, R. E. Alley, and B. J. Curtiss. 1987. "AIS-2 Radiometry and a Comparison of Methods for the Recovery of Ground Reflectance." In *Proceedings of the 3rd airborne imaging spectrometer data analysis workshop*, Pasadena, CA, USA.
- Coops, N. C., M.-L. Smith, M. E. Martin, and S. V. Ollinger. 2003. "Prediction of Eucalypt Foliage Nitrogen Content from Satellite-Derived Hyperspectral Data." *IEEE Transactions on Geoscience and Remote Sensing* 41 (6): 1338–1346. <https://doi.org/10.1109/TGRS.2003.813135>.
- Cortes, C., and V. Vapnik. 1995. "Support-Vector Networks." *Machine Learning* 20 (3): 273–297. <https://doi.org/10.1007/BF00994018>.
- Curran, P. J. 1989. "Remote Sensing of Foliar Chemistry." *Remote Sensing of Environment* 30 (3): 271–278. <https://doi.org/10.1016/0034-42578990069-2>.
- Du, H., R. C. A. Fuh, J. Li, L. A. Corkan, and J. S. Lindsey. 1998. "PhotochemCad#: A Computer-Aided Design and Research Tool in Photochemistry." *Photochemistry and Photobiology* 68 (2): 141–142. <https://doi.org/10.1111/j.1751-1097.1998.tb02480.x>.
- Fourty, T., F. Baret, S. Jacquemoud, G. Schmuck, and J. Verdebout. 1996. "Leaf Optical Properties with Explicit Description of Its Biochemical Composition: Direct and Inverse Problems." *Remote Sensing of Environment* 56 (2): 104–117. <https://doi.org/10.1016/0034-42579500234-0>.
- Gholizadeh, H., M. S. Friedman, N. A. McMillan, W. M. Hammond, K. Hassani, A. V. Sams, M. D. Charles, D. R. Garrett, O. Joshi, and R. G. Hamilton. 2022. "Mapping Invasive Alien Species in Grassland Ecosystems Using Airborne Imaging Spectroscopy and Remotely Observable Vegetation Functional Traits." *Remote Sensing of Environment* 271:112887. <https://doi.org/10.1016/j.rse.2022.112887>.
- Gholizadeh, H., S. M. Robeson, and A. F. Rahman. 2015. "Comparing the Performance of Multispectral Vegetation Indices and Machine-Learning Algorithms for Remote Estimation of Chlorophyll Content: A Case Study in the Sundarbans Mangrove Forest." *International Journal of Remote Sensing* 36 (12): 3114–3133. <https://doi.org/10.1080/01431161.2015.1054959>.
- Guyot, G., F. Baret, and D. Major. 1988. "High Spectral Resolution: Determination of Spectral Shifts Between the Red and Near Infrared." *International Archives of Photogrammetry and Remote Sensing* 11: 740–760. <https://doi.org/10.1029/JB095iB08p12653>

- Haboudane, D., J. R. Miller, N. Tremblay, P. J. Zarco-Tejada, and L. Dextraze. 2002. "Integrated Narrow-Band Vegetation Indices for Prediction of Crop Chlorophyll Content for Application to Precision Agriculture." *Remote Sensing of Environment* 81 (2–3): 416–426. <https://doi.org/10.1016/S0034-42570200018-4>.
- Hank, T. B., K. Berger, H. Bach, J. G. Clevers, A. Gitelson, P. Zarco-Tejada, and W. Mauser. 2019. "Spaceborne Imaging Spectroscopy for Sustainable Agriculture: Contributions and Challenges." *Surveys in Geophysics* 40 (3): 515–551. <https://doi.org/10.1007/s10712-018-9492-0>.
- Hansen, P., and J. Schjoerring. 2003. "Reflectance Measurement of Canopy Biomass and Nitrogen Status in Wheat Crops Using Normalized Difference Vegetation Indices and Partial Least Squares Regression." *Remote Sensing of Environment* 86 (4): 542–553. <https://doi.org/10.1016/S0034-42570300131-7>.
- Hassani, K., H. Gholizadeh, S. Taghvaeian, V. Natalie, J. Carpenter, and J. Jacob. 2023. "Application of UAS-Based Remote Sensing in Estimating Winter Wheat Phenotypic Traits and Yield During the Growing Season." *PFG – Journal of Photogrammetry, Remote Sensing and Geoinformation Science* 91 (2): 1–14. <https://doi.org/10.1007/s41064-022-00229-5>.
- He, L., X. Song, W. Feng, B.-B. Guo, Y.-S. Zhang, Y.-H. Wang, C.-Y. Wang, and T.-C. Guo. 2016. "Improved Remote Sensing of Leaf Nitrogen Concentration in Winter Wheat Using Multi-Angular Hyperspectral Data." *Remote Sensing of Environment* 174:122–133. <https://doi.org/10.1016/j.rse.2015.12.007>.
- Houborg, R., J. B. Fisher, and A. K. Skidmore. 2015. "Advances in Remote Sensing of Vegetation Function and Traits." *International Journal of Applied Earth Observation and Geoinformation* 43:1–6. <https://doi.org/10.1016/j.jag.2015.06.001>.
- Inoue, Y., R. Darvishzadeh, and A. Skidmore. 2018. "Hyperspectral Assessment of Ecophysiological Functioning for Diagnostics of Crops and Vegetation." In *Biophysical and Biochemical Characterization and Plant Species Studies*, 25–71. CRC Press.
- Jay, S., F. Maupas, R. Bendoula, and N. Gorretta. 2017. "Retrieving LAI, Chlorophyll and Nitrogen Contents in Sugar Beet Crops from Multi-Angular Optical Remote Sensing: Comparison of Vegetation Indices and PROSAIL Inversion for Field Phenotyping." *Field Crops Research* 210:33–46. <https://doi.org/10.1016/j.fcr.2017.05.005>.
- Jaynes, D., T. Colvin, D. Karlen, C. Cambardella, and D. Meek. 2001. "Nitrate Loss in Subsurface Drainage as Affected by Nitrogen Fertilizer Rate." *Journal of Environmental Quality* 30 (4): 1305–1314. <https://doi.org/10.2134/jeq2001.3041305x>.
- Jiang, J., Z. Zhang, Q. Cao, Y. Liang, B. Krienke, Y. Tian, Y. Zhu, W. Cao, and X. Liu. 2020. "Use of an Active Canopy Sensor Mounted on an Unmanned Aerial Vehicle to Monitor the Growth and Nitrogen Status of Winter Wheat." *Remote Sensing* 12 (22): 3684. <https://doi.org/10.3390/rs12223684>.
- Kalacska, M., M. Lalonde, and T. Moore. 2015. "Estimation of Foliar Chlorophyll and Nitrogen Content in an Ombrotrophic Bog from Hyperspectral Data: Scaling from Leaf to Image." *Remote Sensing of Environment* 169:270–279. <https://doi.org/10.1016/j.rse.2015.08.012>.
- Kokaly, R. F., G. P. Asner, S. V. Ollinger, M. E. Martin, and C. A. Wessman. 2009. "Characterizing Canopy Biochemistry from Imaging Spectroscopy and Its Application to Ecosystem Studies." *Remote Sensing of Environment* 113:S78–S91. <https://doi.org/10.1016/j.rse.2008.10.018>.
- Kokaly, R. F., and A. K. Skidmore. 2015. "Plant Phenolics and Absorption Features in Vegetation Reflectance Spectra Near 1.66 Mm." *International Journal of Applied Earth Observation and Geoinformation* 43:55–83. <https://doi.org/10.1016/j.jag.2015.01.010>.
- Liang, L., L. Di, T. Huang, J. Wang, L. Lin, L. Wang, and M. Yang. 2018. "Estimation of Leaf Nitrogen Content in Wheat Using New Hyperspectral Indices and a Random Forest Regression Algorithm." *Remote Sensing*, 10(12), 1940.
- Li, J., A. N. Veeranampalayam-Sivakumar, M. Bhatta, N. D. Garst, H. Stoll, P. Stephen Baenziger, V. Belamkar, R. Howard, Y. Ge, and Y. Shi. 2019. "Principal Variable Selection to Explain Grain Yield Variation in Winter Wheat from Features Extracted from UAV Imagery." *Plant Methods* 15 (1): 123. <https://doi.org/10.1186/s13007-019-0508-7>.

- Lollato, R. P., B. M. Figueiredo, J. S. Dhillon, D. B. Arnall, and W. R. Raun. 2019. "Wheat Grain Yield and Grain-Nitrogen Relationships as Affected by N, P, and K Fertilization: A Synthesis of Long-Term Experiments." *Field Crops Research* 236:42–57. <https://doi.org/10.1016/j.fcr.2019.03.005>.
- Lynch, J. M., and D. M. Barbano. 1999. "Kjeldahl Nitrogen Analysis as a Reference Method for Protein Determination in Dairy Products." *Journal of AOAC International* 82 (6): 1389–1398. <https://doi.org/10.1093/jaoac/82.6.1389>.
- Masclaux-Daubresse, C., F. Daniel-Vedele, J. Dechorgnat, F. Chardon, L. Gaufichon, and A. Suzuki. 2010. "Nitrogen Uptake, Assimilation and Remobilization in Plants: Challenges for Sustainable and Productive Agriculture." *Annals of Botany* 105 (7): 1141–1157. <https://doi.org/10.1093/aob/mcq028>.
- Milford, G., T. Pocock, J. RILEY, and A. Messum. 1985. "An Analysis of Leaf Growth in Sugar Beet. III. Leaf Expansion in Field Crops." *Annals of Applied Biology* 106 (1): 187–203. <https://doi.org/10.1111/j.1744-7348.1985.tb03108.x>.
- Miphokasap, P., and W. Wannasiri. 2018. "Estimations of Nitrogen Concentration in Sugarcane Using Hyperspectral Imagery." *Sustainability* 10 (4): 1266. <https://doi.org/10.3390/su10041266>.
- Naftel, J. A. 1931. "The Absorption of Ammonium and Nitrate Nitrogen by Various Plants at Different Stages of Growth 1." *Agronomy Journal* 23 (2): 142–158. <https://doi.org/10.2134/agronj1931.00021962002300020005x>.
- Näsi, R., N. Viljanen, J. Kaivosoja, K. Alhonoja, T. Hakala, L. Markelin, and E. Honkavaara. 2018. "Estimating Biomass and Nitrogen Amount of Barley and Grass Using UAV and Aircraft Based Spectral and Photogrammetric 3D Features." *Remote Sensing* 10 (7): 1082. <https://doi.org/10.3390/rs10071082>.
- Nigon, T. J., D. J. Mulla, C. J. Rosen, Y. Cohen, V. Alchanatis, J. Knight, and R. Rud. 2015. "Hyperspectral Aerial Imagery for Detecting Nitrogen Stress in Two Potato Cultivars." *Computers and Electronics in Agriculture* 112:36–46. <https://doi.org/10.1016/j.compag.2014.12.018>.
- Pullanagari, R., M. Dehghan-Shoar, I. J. Yule, and N. Bhatia. 2021. "Field Spectroscopy of Canopy Nitrogen Concentration in Temperate Grasslands Using a Convolutional Neural Network." *Remote Sensing of Environment* 257:112353. <https://doi.org/10.1016/j.rse.2021.112353>.
- Rasmussen, C. E. 2003. "Gaussian Processes in Machine Learning." In *Summer School on Machine Learning*, 63–71. Berlin: Springer. https://doi.org/10.1007/978-3-540-28650-9_4.
- Raun, W. R., J. Dhillon, L. Aula, E. Eickhoff, G. Weymeyer, B. Figueirde, T. Lynch, P. Omara, E. Nambi, and F. Oyebiyi. 2019. "Unpredictable Nature of Environment on Nitrogen Supply and Demand." *Agronomy Journal* 111 (6): 2786–2791. <https://doi.org/10.2134/agronj2019.04.0291>.
- Rouse, J. 1974. Monitoring the Vernal Advancement of Retrogradation of Natural Vegetation. NASA/GSFC, type III, final report, greenbelt, MD, 371.
- Skiba, U., and B. Rees. 2014. "Nitrous Oxide, Climate Change and Agriculture." *CAB Reviews* 9 (10): 1–7. <https://doi.org/10.1079/PAVSNNR20149010>.
- Townsend, P. A., J. R. Foster, R. A. Chastain, and W. S. Currie. 2003. "Application of Imaging Spectroscopy to Mapping Canopy Nitrogen in the Forests of the Central Appalachian Mountains Using Hyperion and AVIRIS." *IEEE Transactions on Geoscience and Remote Sensing* 41 (6): 1347–1354. <https://doi.org/10.1109/TGRS.2003.813205>.
- Ustin, S. L., and J. A. Gamon. 2010. "Remote Sensing of Plant Functional Types." *New Phytologist* 186 (4): 795–816. <https://doi.org/10.1111/j.1469-8137.2010.03284.x>.
- Ustin, S. L., A. A. Gitelson, S. Jacquemoud, M. Schaepman, G. P. Asner, J. A. Gamon, and P. Zarco-Tejada. 2009. "Retrieval of Foliar Information About Plant Pigment Systems from High Resolution Spectroscopy." *Remote Sensing of Environment* 113:S67–S77. <https://doi.org/10.1016/j.rse.2008.10.019>.
- Wang, Z., A. Chlus, R. Geygan, Z. Ye, T. Zheng, A. Singh, J. J. Couture, J. Cavender-Bares, E. L. Kruger, and P. A. Townsend. 2020. "Foliar Functional Traits from Imaging Spectroscopy Across Biomes in Eastern North America." *New Phytologist* 228 (2): 494–511. <https://doi.org/10.1111/nph.16711>.
- Wang, F., J. Huang, Y. Wang, Z. Liu, D. Peng, and F. Cao. 2013. "Monitoring Nitrogen Concentration of Oilseed Rape from Hyperspectral Data Using Radial Basis Function." *International Journal of Digital Earth* 6 (6): 550–562. <https://doi.org/10.1080/17538947.2011.628414>.

- Weiss, M., F. Jacob, and G. Duveiller. 2020. "Remote Sensing for Agricultural Applications: A Meta-Review." *Remote Sensing of Environment* 236:111402. <https://doi.org/10.1016/j.rse.2019.111402>.
- White, C. M., D. M. Finney, A. R. Kemanian, and J. P. Kaye. 2021. "Modeling the Contributions of Nitrogen Mineralization to Yield of Corn." *Agronomy Journal* 113 (1): 490–503. <https://doi.org/10.1002/agj2.20474>.
- Wold, S., M. Sjöström, and L. Eriksson. 2001. "PLS-Regression: A Basic Tool of Chemometrics." *Chemometrics and Intelligent Laboratory Systems* 58 (2): 109–130. [https://doi.org/10.1016/S0169-7439\(01\)00155-1](https://doi.org/10.1016/S0169-7439(01)00155-1).
- Wright, I. J., P. B. Reich, M. Westoby, D. D. Ackerly, Z. Baruch, F. Bongers, J. Cavender-Bares, T. Chapin, J. H. Cornelissen, and M. Diemer. 2004. "The Worldwide Leaf Economics Spectrum." *Nature* 428 (6985): 821–827. <https://doi.org/10.1038/nature02403>.
- Yao, W., M. van Leeuwen, P. Romanczyk, D. Kelbe, and J. van Aardt. 2015. "Assessing the Impact of Sub-Pixel Vegetation Structure on Imaging Spectroscopy via Simulation. In V. Miguel & F.A. Kruse (Eds.), *Algorithms and Technologies for Multispectral, Hyperspectral, and Ultraspectral Imagery XXI*, Vol. 9472, 546–552. Baltimore, MA, USA: SPIE.
- Zhou, K., T. Cheng, Y. Zhu, W. Cao, S. L. Ustin, H. Zheng, X. Yao, and Y. Tian. 2018. "Assessing the Impact of Spatial Resolution on the Estimation of Leaf Nitrogen Concentration Over the Full Season of Paddy Rice Using Near-Surface Imaging Spectroscopy Data." *Frontiers in Plant Science* 9:964. <https://doi.org/10.3389/fpls.2018.00964>.